VORTICITY TRANSPORT IN HUMAN AIRWAY MODEL

Andras Nemes
Dept. of Aerospace Engineering & Mechanics
University of Minnesota
Minneapolis, MN 55455, USA
nemesa@umn.edu

Tristan Van de Moortele
Dept. of Aerospace Engineering & Mechanics
University of Minnesota
Minneapolis, MN 55455, USA
vande935@umn.edu

Sahar Jalal
Dept. of Aerospace Engineering & Mechanics
University of Minnesota
Minneapolis, MN 55455, USA
jalal011@umn.edu

Filippo Coletti
Dept. of Aerospace Engineering & Mechanics
University of Minnesota
Minneapolis, MN 55455, USA
fcoletti@umn.edu

ABSTRACT

Many previous studies concerned with respiratory fluid mechanics have simplistically assumed steady and laminar flow. Above a certain ventilation frequency, the unsteady nature of the respiratory flow becomes apparent, and inhalation and exhalation cannot be approximated as quasi-stationary processes. Moreover, due to the geometrical structure of the bronchial tree, flow unsteadiness and transition to turbulence can incept even at Reynolds numbers usually considered laminar in parallel flows. Here we investigate the primary features of the oscillatory flow through a 3D printed double bifurcation model that reproduces, in an idealized manner, the self-similar branching of the human bronchial tree. We consider Reynolds and Womersley numbers relevant to physiological conditions between the trachea and the lobar bronchi. Three-component, three-dimensional velocity fields are acquired at multiple phases of the ventilation cycle using Magnetic Resonance Velocimetry (MRV). The phase-averaged volumetric data provide a detailed description of the flow topology, characterizing the main secondary flow structures and their spatio-temporal evolution. We also perform two-dimensional by Particle Image Velocimetry (PIV) for the steady inhalation case at a Reynolds number Re = 2000. PIV is carried out by matching the refractive index of the 3D printing resin with a novel combination of anise oil and mineral oil. The instantaneous measurements reveal unsteadiness of the separating unsteady flow in the bifurcation, and the ensemble averages show a clear Reynolds stress pattern indicating that the flow is turbulent at the first bronchial bifurcation already at this relatively low Reynolds number.

INTRODUCTION

The human respiratory system is structured as a network of branching airways. The trachea splits in the two main bronchioles, which successively bifurcate about sixteen more times down to the terminal bronchi, followed by roughly six generations of alveolar ducts involved in the gas exchange (Kleinstreuer & Zhang 2010). While the actual anatomy is fairly complex and varies between different subjects, general features have been long identified which are remarkably consistent: at the i^{th} bronchial generation, the daughter-to-mother branch diameter ratio is $h = D_{i+1}/D_i \approx 0.8$, the length-to-diameter ratio of each branch is $Li/Di \approx 3.5$, and the bifurcation angle is $\theta \approx 60\text{-}70°$ (Weibel 1997). Such proportions minimize the through-flow time during the respiration process and the energy expenditure in bifurcating flow systems, and therefore canonical airway models with such characteristics have been extensively studied. The most classic case is the planar version of the Weibel A model (Weibel 1963), in which the branches consist of circular tubes that bifurcate symmetrically and lay on the same plane. Despite the simplicity of such representation, this has been shown to capture many key aspects of the respiratory airflow both in inspiratory and expiratory mode. Above a certain ventilation frequency, the unsteady nature of the respiration becomes apparent, and inhalation and exhalation cannot be approximated as quasi-stationary processes. This is especially important in the upper and central airways, where length and velocity scales are larger, making inertia and acceleration effects dominant over viscous dissipation. In this study we experimentally investigate the primary features of the oscillatory flow through a symmetric double bifurcation, which models the self-similar branching of the human bronchial tree. The focus is on the generation and transport of vorticity during the respiratory cycle/ This process is at the root of the strong secondary flows and characterizes the instantaneous shear layers in this complex, unsteady flow.

EXPERIMENTAL METHODOLOGY

The airway geometry we investigate is a planar Weibel A double bifurcation, and it replicates the model studied numerically by Comer et al. (2001). A schematic of the geometry with dimensions is given in Fig. 1, along with a 3D rendering. Similar (when not identical) geometries have been used in several previous experimental and numerical studies (Zhang and Kleinstreuer 2002, Longest and Vinchurkar 2007, Fresconi and Prasad 2007, among others). This specific model was chosen because of the full description of the geometry and velocity fields reported by Comer et al. (2001). Their study suggests that fine details as the rounding radius at the carina have a moderate effect as compared to more macroscopic features such as the bifurcation angle. We label the three branching generation G0 (mother branch, receiving the inflow), G1 (daughter branches, after the first bifurcation), and G2 (granddaughter branches, after the second bifurcation). Typical airway labeling schemes use G0 for the trachea, G1 for the main bronchi, etc., but here we do not strictly associate the mother branch with the trachea. Rather, assuming a quasi-

homothetic airway model, this geometry may represent a different location in the airway tree depending on the Reynolds number. We investigate a range of Reynolds and Womersley numbers relevant to physiological conditions between the trachea and the lobar bronchi. We define the Reynolds number defined as $Re = U_0D0/\nu$, where D_0 and U_0 are the diameter and peak bulk velocity at G0, and ν is the kinematic viscosity. The Womersley number is defined as $Wo = D_0/2\sqrt{(\omega/\nu)}$, where ω is the angular frequency of oscillation. Here we present measurements at Wo = 3 and peak Reynolds number Re = 2000.

The airway geometry we investigate is a planar Weibel A double bifurcation, and it replicates the model studied numerically by Comer et al. (2001), see Fig. 1. We label the three branching generation G0 (mother branch, receiving the inflow), G1 (daughter branches, after the first bifurcation), and G2 (granddaughter branches, after the second bifurcation). The model is 3D printed by stereolithography with a layer thickness of 25 micron, which warrants high geometric precision and hydrodynamic smoothness. We investigate a range of Reynolds and Womersley numbers relevant to physiological conditions between the trachea and the lobar bronchi. We define the Reynolds number defined as $Re = U_0D0/\nu$, where D_0 and U_0 are the diameter and peak bulk velocity at G0, and ν is the kinematic viscosity. The Womersley number is defined as $Wo = D_0/2\sqrt{(\omega/\nu)}$, where ω is the angular frequency of oscillation. To this end we use a in-house built oscillatory pump. For the present study we impose a peak Reynolds number Re = 2000 and vary the Womersely number in the range Wo = 1 - 12, spanning conditions from slow breathing to high frequency ventilation. Here we show results for the Wo = 3 case.

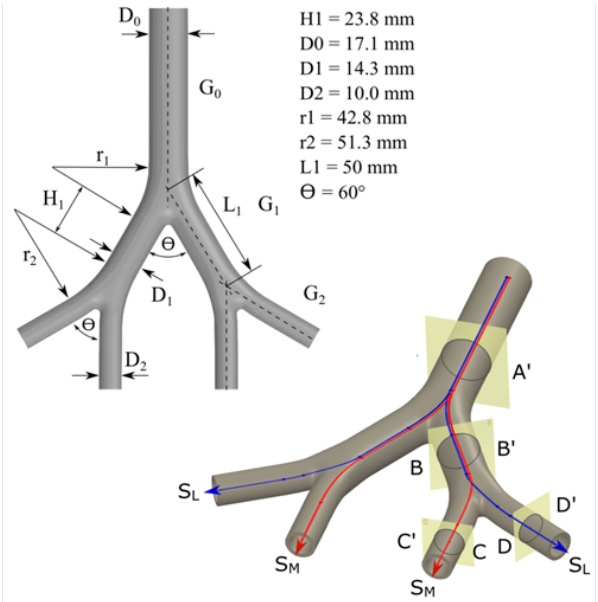

Fig. 1. Schematic of the geometry of the double bifurcation.

A physical model of the bifurcation is 3D printed using a clear resin (Waterhsed XC 11122), and is hermetically sealed to plastic tubing that connect it to an oscillatory pump. The pump consists of a piston sliding through a 8 cm diameter cylinder, and driven by a numerically controlled stepper motor which imposes the desired sinusoidal waveform. Three-component, three-dimensional velocity fields are acquired at multiple phases of the ventilation cycle using Magnetic Resonance Velocimetry (MRV). For maximum signal in the MRV measurements, the working fluid is water with 0.06 mol/L of CuSO4. A 3 Tesla Siemens MRI scanner (Fig. 2) is employed. Velocity data are obtained using the method described by Elkins et al. (2007), with the signaling and data acquisition sequence from Markl. et al. (2012). Three-dimensional, three-component (3D-3C) velocities are obtained on a uniform Cartesian grid at a resolution of 0.6 mm. The field of view is 153.6 by 307.2 by 26.4 mm^3 and includes both the fluid and the solid walls of the test section. By gating the MRI signal, 10 phased-averaged velocity fields are obtained within the respiration cycle. The procedure is similar to the one used by Banko et al. (2016) who studied the oscillatory flow in a subject-specific airway model. Figure 3 shows the excellent agreement between the imposed waveform and the flow rate measured by MRV at a cross-section in generation G0.

Fig. 2. The 3 Tesla Siemens MRI scanner used for the MRV measurements, with the model inserted in the head coil.

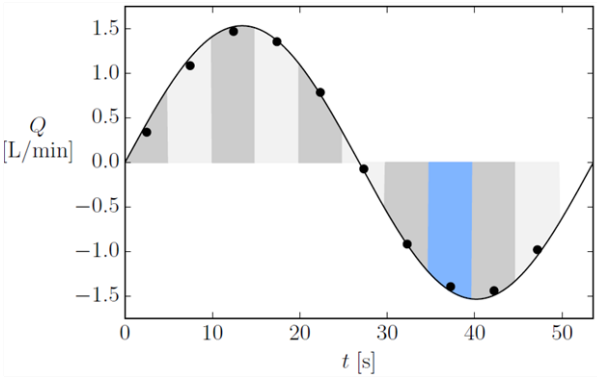

Fig. 3 Flow rate measured by MRV at the trachea (symbols), compared to the ideal sinusoidal waveform imposed by the oscillatory piston pump.

Three-component, three-dimensional velocity fields are acquired at multiple phases of the ventilation cycle using Magnetic Resonance Velocimetry (MRV). For maximum signal in the MRV measurements, the working fluid is water with 0.06 mol/L of CuSO4. A 3 Tesla Siemens MRI scanner is employed. Velocity data are obtained using the method described by Elkins et al. (2007), with the signaling and data acquisition sequence from Markl. et al. (2012). Three-dimensional, three-component (3D-3C) velocities are obtained on a uniform Cartesian grid at a resolution of 0.6 mm. The field of view is 153.6 by 307.2 by 26.4 mm^3 and includes both the

fluid and the solid walls of the test section. By gating the MRI signal, 10 phased-averaged velocity fields are obtained within the respiration cycle. The procedure is similar to the one used by Banko et al. (2016) who studied the oscillatory flow in a subject-specific airway model. Excellent agreement is found between the imposed waveform and the flow rate measured by MRV through the mother branch G0.

Additionally, 2D velocity fields are obtained by Particle Image Velocimetry (PIV) along the symmetry plane of the bifurcation. The PIV system includes an Nd:YAG laser operated at 3 Hz and a 4 Megapixel CCD camera. Refractive index matching between the 3D printed model and the working fluid is achieved using a 57%-43% mixture by volume of anise oil and mineral oil (n = 1.5114, as measured by an optical refractometer). In the past Butscher et al. (2012) obtained PIV measurements in a 3D printed model manufactured with the same material as ours using anisole, which however is expensive and dissolves the material relatively quickly. Hafeli et al. (2014) used a tunable and less aggressive mixture of NaI and ZnI_2, which however oxidizes and looses clarity in contact with air. The mixture of anise oil and mineral oil used here is not aggressive to WaterShed, it is obtained with relatively inexpensive products, and does not oxidize when exposed to air. Figure 4 shows an example of PIV image obtained thanks to the refractive index matching.

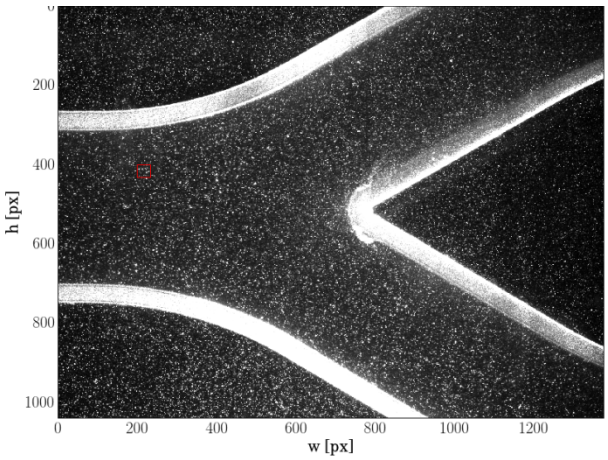

Fig. 4. Sample image from refractive-index-matched PIV run.

RESULTS

The measurements along the bifurcation symmetry plane close to peak inspiration and peak expiration show very non-homogeneous velocity (Fig. 5). This is due to the significant flow inertia at the considered Reynolds number, which produces jet-like patterns at each bifurcation. Moreover, due to the curvature of the branches, secondary flow motions are set up by Dean mechanism, and give raise to regions of strong streamwise vorticity (Fig. 6). During inspiration, as the flow is divided at the carina between G0 and G1 branches, two main counter-rotating vortices are formed. Likewise, during expiration, the flow from both pairs of G2 branches merges in the respective G1 branches, resulting in a quadruplet of counter-rotating vortices. The two quadruplets of streamwise vortices in both generations G1 merge in generation G0, and produce the pattern displayed in Fig. 7: four counter-rotating vortices occupy the core of the airway, and each one is associated to structures of opposite vorticity embedded in the near-wall region. During inspiration, the flow in the medial G2 branches is very different from the flow in the lateral G2 branches (Fig. 8). In the latter, the Dean mechanism causes a pair of streamwise vortices, while in the former the vortices from G1 branches survive and coexist with Dean-type vortices, creating a quadruplet of vortices.

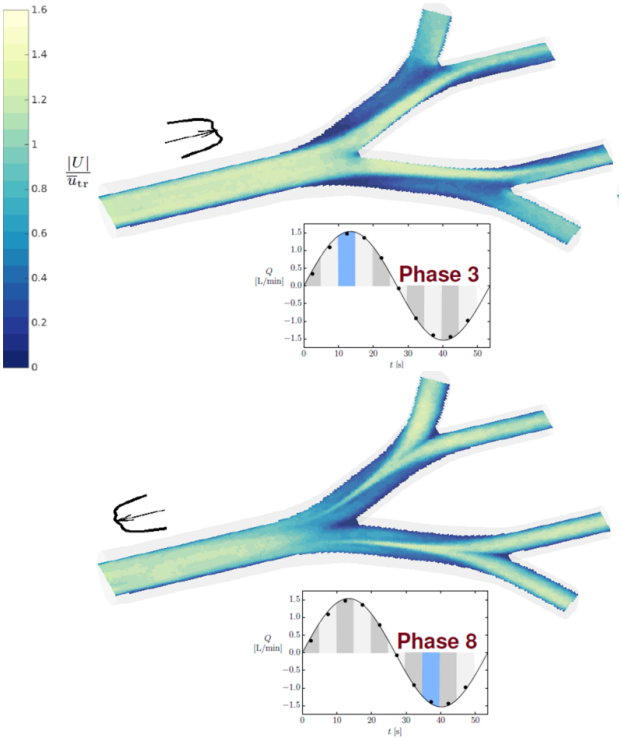

Fig. 5: Contours of velocity magnitude measured by MRV close to peak inspiration (top) and close to peak expiration (bottom) at the symmetry plane.

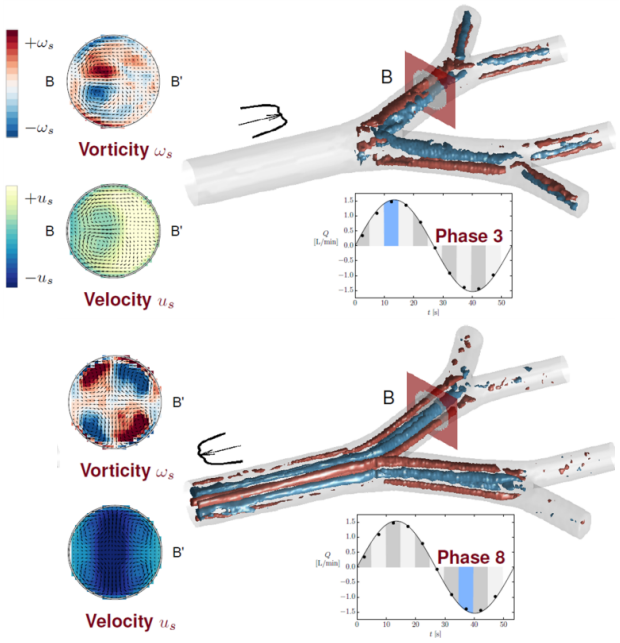

Fig. 6. Contours of streamwise velocity and vorticity measured by MRV close to peak inspiration (top) and close to peak expiration (bottom) at a cross section of generation G1.

Isosurfaces of positive and negative streamwise vorticity are also shown.

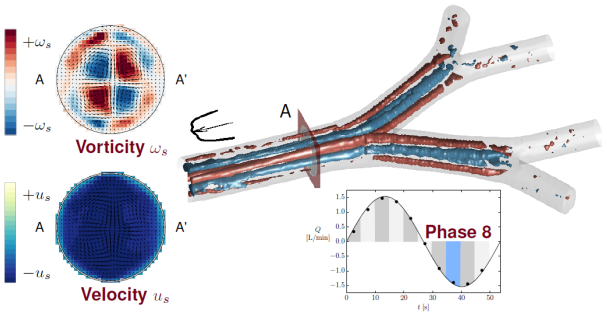

Fig. 7. Contours of streamwise velocity and vorticity measured by MRV close to peak exhalation at a cross section of generation G0. Isosurfaces of positive and negative streamwise vorticity are also shown.

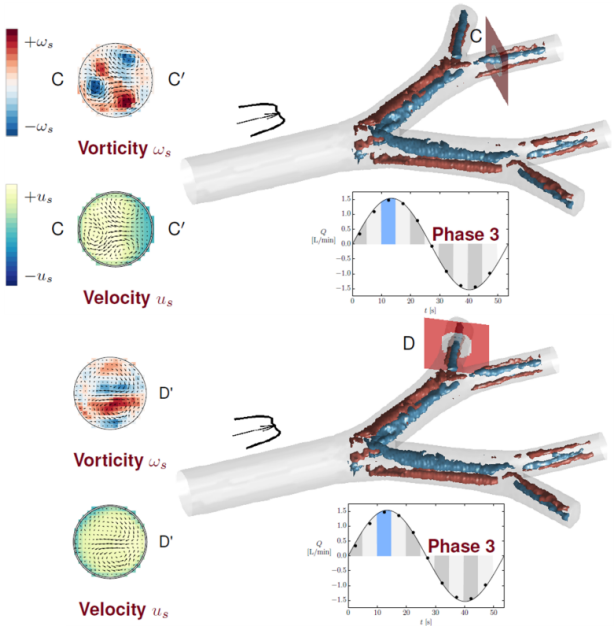

Fig. 8. Contours of streamwise velocity and vorticity measured by MRV close to peak inspiration at a cross section of generation G2, for the medial (top) and lateral (bottom) branch. Isosurfaces of positive and negative streamwise vorticity are also shown.

PIV measurements provide mean velocity field (obtained from 1000 realizations) in good agreement with MRV measurements, both run at steady inflow conditions (Fig. 9). The Reynolds stress fields from PIV indicate that transition to unsteady/turbulent regime has already occurred at Re = 2000, for which most previous numerical studies assumed laminar flow, see Fig. 10. While the flow is indeed laminar and follows a Poiseuille profile in the entry pipe, intense velocity fluctuations are created by the shear layers of the jet-like flow expanding from G0 into the first bifurcation. These are even intensified along the G1 branches, likely due in the secondary flows bringing together fast-moving and slow-moving fluid and enhancing the turbulent momentum transport. The clear pattern of intense Reynolds stresses along the shear layers suggest that the flow is actually turbulent.

The instantaneous PIV realizations suggest that the unsteadiness in the flow may be, in part, associated to a large-scale flapping motion, with substantial fraction of the momentum oscillating from the right to the left daughter branch (Fig. 11). The details of this process are still under investigation, as well as its coupling with other instabilities in the system associated to the shear layers in the bifurcation.

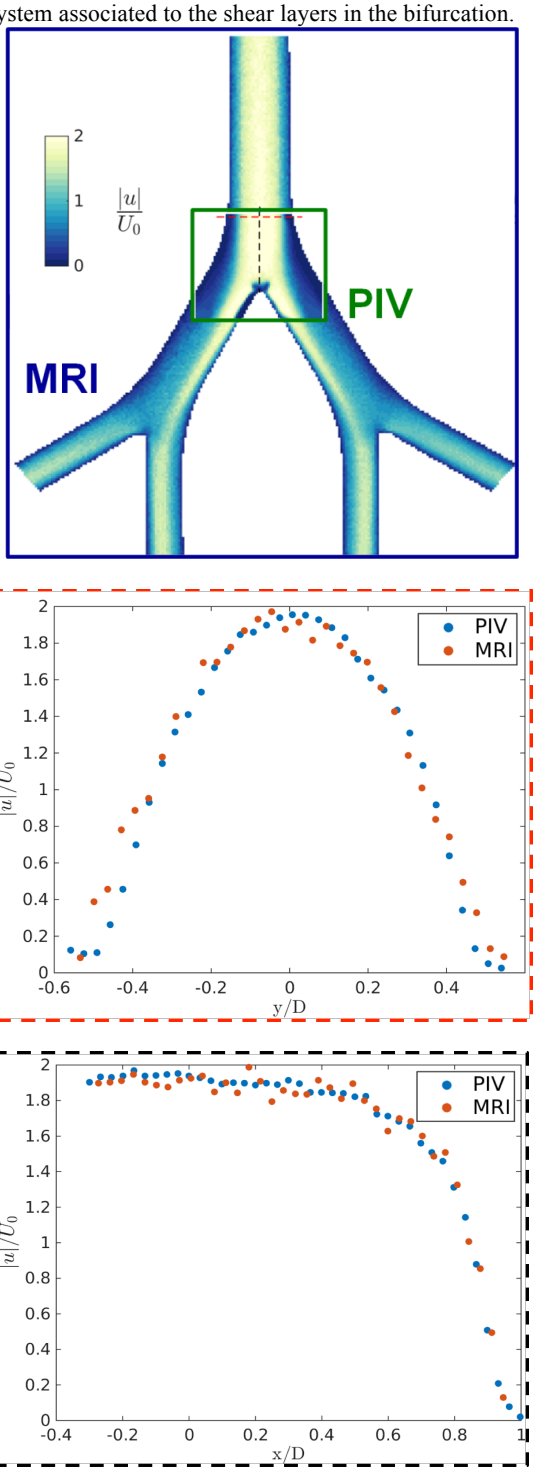

Fig. 9. Comparison between MRV and PIV along the symmetry plane (top), with line plot comparisons along two segments at the bifurcation, in streamwise (middle) and tranverse (bottom) direction. Data obtained for steady inflow conditions at Re = 2000.

CONCLUSIONS

MRV allows to reconstruct the full three-dimensional velocity field at various phases during the respiration cycle. Most

previous measurements had focused on very low Reynolds numbers and found flow features dominated Dean vortices driven by the local curvatures (e.g. Fresconi and Prasad 2007). Here we show how the vortices generated in a given bifurcation can survive into further branching generations, so that the secondary velocity field in each branch can be strongly influenced by the upstream flow. This is apparent looking at the patterns of streamwise vorticity extending through successive bifurcations. For the steady inspiration case, PIV agrees well with MRV obtained at the same conditions, and adds valuable information in terms of Reynolds stresses. In particular, it indicates that transition to unsteady/turbulent regime has already occurred at Re = 2000, for which most previous numerical studies assumed laminar flow. The instantaneous

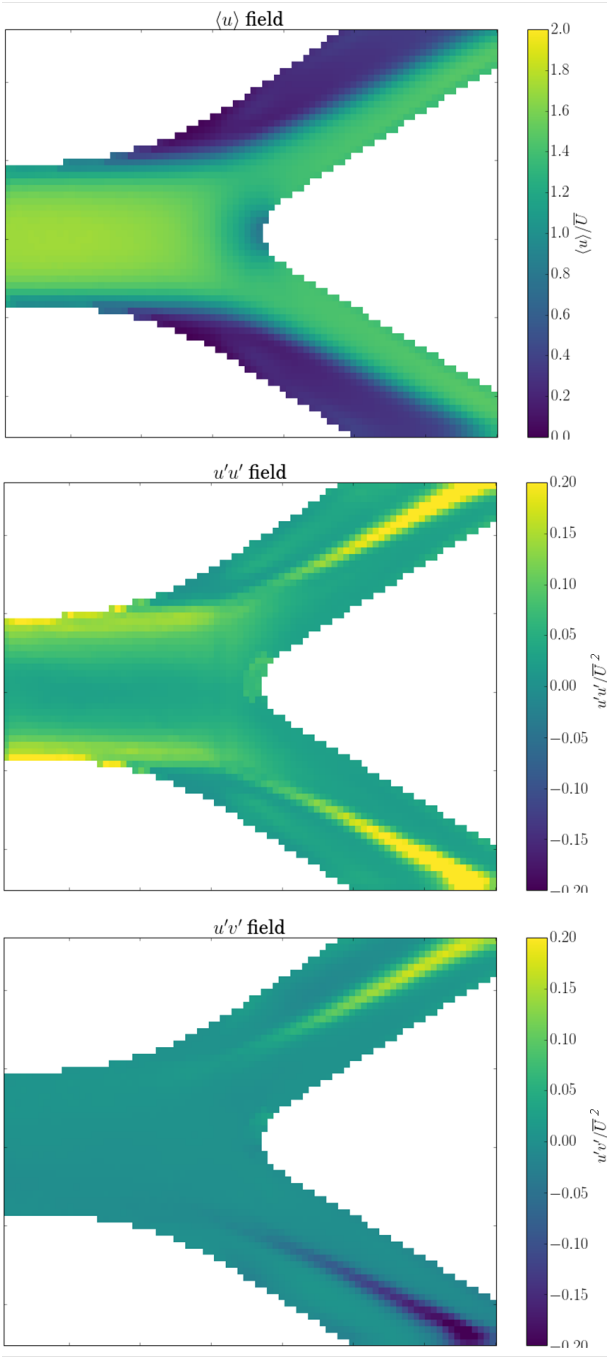

Fig. 10. PIV measurements along the bifurcation symmetry plane: mean streamwise velocity (top), streamwise Reynolds stresses (middle), and Reynolds shear stresses (bottom).

velocity fields reveal the unsteady nature of the flow even at relatively low Reynolds numbers. This may have far reaching consequences from the clinical standpoint, in terms of both pressure losses and inhaled particle transport in the airways.

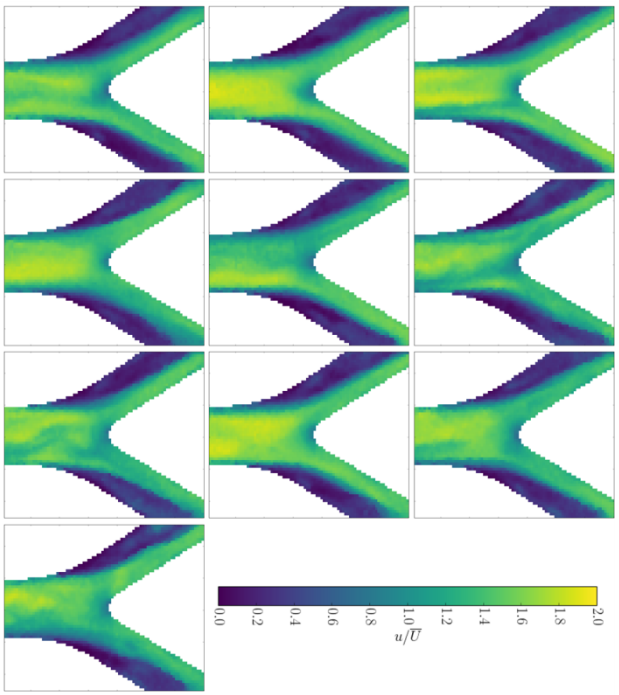

Fig. 11. Series of successive instantaneous streamwise velocity fields, showing large scale flapping motion between the sister branches of the bifurcation.

REFERENCES

Banko A., Coletti F., Elkins C.J., Eaton, J.K. (2016) "Oscillatory Flow in the Human Airways from the Mouth through Several Bronchial Generations". Int. J. Heat Fluid Flow, in press

Butscher, D., Hutter, C., Kuhn, S., & von Rohr, P. R. (2012). Particle image velocimetry in a foam-like porous structure using refractive index matching: a method to characterize the hydrodynamic performance of porous structures. Experiments in fluids, 53(4), 1123-1132.

Comer, J. K., Kleinstreuer, C., & Zhang, Z. (2001). Flow structures and particle deposition patterns in double-bifurcation airway models. Part 1. Air flow fields. *Journal of Fluid Mechanics*, *435*, 25-54.

Elkins, C. J., & Alley, M. T. (2007). Magnetic resonance velocimetry: applications of magnetic resonance imaging in the measurement of fluid motion. *Experiments in Fluids*, *43*(6), 823-858.

Fresconi, F. E., & Prasad, A. K. (2007). Secondary velocity fields in the conducting airways of the human lung. *Journal of biomechanical engineering*,*129*(5), 722-732.

Grotberg, J. B. (2001). Respiratory fluid mechanics and transport processes.*Annual review of biomedical engineering*, *3*(1), 421-457.

Häfeli, R., Altheimer, M., Butscher, D., & von Rohr, P. R. (2014). PIV study of flow through porous structure using refractive index matching. Experiments in Fluids, 55(5), 1-13.

Kleinstreuer, C., & Zhang, Z. (2010). Airflow and particle transport in the human respiratory system. *Annual Review of Fluid Mechanics*, *42*, 301-334.

Markl, M., Frydrychowicz, A., Kozerke, S., Hope, M., & Wieben, O. (2012). 4D flow MRI. *Journal of Magnetic Resonance Imaging*, *36*(5), 1015-1036.

Pedley, T. J. (1977). Pulmonary fluid dynamics. *Annual Review of Fluid Mechanics*, *9*(1), 229-274.

Weibel, E. R. (1963). Principles and methods for the morphometric study of the lung and other organs. *Laboratory investigation; a journal of technical methods and pathology*, *12*, 131.

Weibel, E. R. (1997). Design of airways and blood vessels considered as branching tree, Chapter 74. *The Lung, RG Crystal, JB West, and PJ Barnes (Eds.), Lippencott-Raven Inc., Philadelphia*.

Zhang, Z., & Kleinstreuer, C. (2002). Transient airflow structures and particle transport in a sequentially branching lung airway model. *Physics of Fluids (1994-present)*, *14*(2), 862-880.